

# Constraining neutrino oscillation parameters with current solar and atmospheric data

---

**M. Maltoni,**

*Instituto de Física Corpuscular – C.S.I.C./Universitat de València  
Edificio Institutos de Paterna, Apt 22085, E-46071 Valencia, Spain  
E-mail: maltoni@ific.uv.es*

**T. Schwetz,**

*Institut für Theoretische Physik, Universität Wien  
Boltzmanngasse 5, A-1090 Wien, Austria  
E-mail: schwetz@thp.univie.ac.at*

**M. A. Tórtola,**

*Instituto de Física Corpuscular – C.S.I.C./Universitat de València  
Edificio Institutos de Paterna, Apt 22085, E-46071 Valencia, Spain  
E-mail: mariam@ific.uv.es*

**and J. W. F. Valle,**

*Instituto de Física Corpuscular – C.S.I.C./Universitat de València  
Edificio Institutos de Paterna, Apt 22085, E-46071 Valencia, Spain  
E-mail: valle@ific.uv.es*

**ABSTRACT:** We analyse the impact of recent solar and atmospheric data in the determination of the neutrino oscillation parameters, taking into account that both the solar  $\nu_e$  and the atmospheric  $\nu_\mu$  may convert to a mixture of active and sterile neutrinos. In addition to the recent SNO neutral current (NC), spectral and day/night data we add the latest 1496-day solar and 1489-day atmospheric Super-K neutrino data samples. By investigating in detail the impact of the recent SNO NC, spectral and day/night data, we confirm the clear preference of the LMA solution of the solar neutrino problem and obtain that the LOW, VAC, SMA solutions are disfavoured with a  $\Delta\chi^2 = 9, 9, 23$ , respectively. Furthermore, we find that the global solar data constrains the admixture of a sterile neutrino to be less than 45% at 99% C.L.. A pure sterile solution is ruled out with respect to the active one at 99.996% C.L.. By performing an improved fit of the atmospheric data, we also update the corresponding regions of oscillation parameters. We find that the recent atmospheric Super-K (1489-day) and MACRO data have a strong impact on constraining a sterile component in atmospheric oscillations: if the  $\nu_\mu$  is restricted to the atmospheric mass states only a sterile admixture of 16% is allowed at 99% C.L., while a bound of 35% is obtained in the unconstrained case. Pure sterile oscillations are disfavoured with a  $\Delta\chi^2 = 34.6$  compared to the pure active case.

**KEYWORDS:** solar and atmospheric neutrinos, neutrino and Gamma Astronomy, neutrino physics.

---

## Contents

<b>1. Introduction</b>	<b>1</b>
<b>2. Solar neutrinos</b>	<b>3</b>
2.1 Active-sterile solar neutrino oscillations	3
2.2 Data and analysis	3
2.3 Results and discussion	5
<b>3. Atmospheric neutrinos</b>	<b>10</b>
3.1 Active-sterile atmospheric neutrino oscillations	10
3.2 Data and analysis	10
3.3 Results and Discussion	11
<b>4. Conclusions</b>	<b>16</b>

---

## 1. Introduction

Apart from confirming, yet again, the long-standing solar neutrino problem [1, 2, 3, 4, 5], the recent results from the Sudbury Neutrino Observatory (SNO) on neutral current events [6, 7] have given strong evidence that solar neutrinos convert mainly to an active neutrino flavor. In addition, valuable spectral and day/night information has been provided [6, 7]. This adds to the already robust evidence that an extension of the Standard Model of particle physics is necessary in the lepton sector. Although certainly not yet unique, at least for the case of solar neutrinos, which can be accounted well by spin-flavor precession [8] or non-standard neutrino matter interactions [9], the most popular joint explanation of solar and atmospheric experiments is provided by the neutrino oscillations hypothesis, with neutrino mass-squared differences of the order of  $\Delta m_{\text{SOL}}^2 \lesssim 10^{-4}$  eV<sup>2</sup> and  $\Delta m_{\text{ATM}}^2 \sim 2 \times 10^{-3}$  eV<sup>2</sup>, respectively.

In the wake of the recent SNO-NC results we have re-analyzed the global status of current neutrino oscillation data including these and the remaining solar data [1, 2, 3, 4, 5, 6, 7] as well as the current atmospheric [10, 11] samples, including the 1489 days Super

Kamiokande data [12] and the most recent MACRO data [13]. Motivated by the stringent limits from reactor experiments [14] we will adopt an effective two-neutrino approach in which solar and atmospheric analyses decouple. However the effective two-neutrino approach which we will adopt is generalized in the sense that it takes into account that a light sterile neutrino [15, 16, 17, 18, 19, 20], advocated to account for the LSND anomaly [21], may take part in both solar and atmospheric conversions. In other words we will re-evaluate the status of current solar and atmospheric neutrino data and give a new determination of neutrino oscillation parameters assuming that both the solar  $\nu_e$  and the atmospheric  $\nu_\mu$  may convert to a mixture of active and sterile neutrinos. For recent global analyses of all current neutrino oscillation data, including negative short-baseline data and the LSND experiment, in the framework of four-neutrino oscillations see Refs. [22, 23].

The plan of the paper is as follows. In Sec. 2.1 we set our notations for solar oscillations in the presence of active-sterile admixture. This admixture is described by a parameter  $0 \leq \eta_s \leq 1$ . In Sec. 2.2 we briefly describe the solar neutrino data and their analysis. In Sec. 2.3 we present the results of our analysis, aimed at studying the impact of recent solar data in the determination of the solar neutrino oscillation parameters, assuming, as mentioned, that the  $\nu_e$  may convert to a mixture of active and sterile neutrinos. We give the regions of oscillation parameters for different allowed  $\eta_s$  values, display the global behavior of  $\Delta\chi^2_{\text{SOL}}(\Delta m^2_{\text{SOL}})$  and  $\Delta\chi^2_{\text{SOL}}(\theta_{\text{SOL}})$ , calculated with respect to the favored active LMA solution, and evaluate the impact of the SNO NC, spectral and day/night data. Present solar data exhibit a higher degree of rejection against non-LMA and/or non-active oscillation solutions, which we quantify, giving also the absolute goodness of fit (GOF) of various oscillation solutions. Our results are briefly compared with those obtained in other recent analyses [24, 25, 26, 27, 28, 29]. In Sec. 3.1 we set our notations for atmospheric oscillations in the presence of active-sterile admixture. In Sec. 3.2 we briefly describe the atmospheric neutrino data and their analysis. In Sec. 3.3 we describe our results for atmospheric oscillation parameters in an improved global fit of current atmospheric neutrino data. We quantify the impact both of our improved analysis as well as that of the recent data in rejecting against the sterile oscillation hypothesis. We update the corresponding regions of oscillation parameters and display the global behavior of  $\Delta\chi^2_{\text{ATM}}(\Delta m^2_{\text{ATM}})$  and  $\Delta\chi^2_{\text{ATM}}(\theta_{\text{ATM}})$ . We compare the situation before-and-after the recent 1489-day atmospheric Super-K data samples and give the present GOF of the oscillation hypothesis. Finally in Sec. 4 we present our conclusions.

## 2. Solar neutrinos

### 2.1 Active-sterile solar neutrino oscillations

In the following we will analyze solar neutrino data in the general framework of mixed active-sterile neutrino oscillations. In this case the electron neutrino produced in the sun converts into a combination of an active non-electron neutrino  $\nu_x$  (which again is a combination of  $\nu_\mu$  and  $\nu_\tau$ ) and a sterile neutrino  $\nu_s$ :

$$\nu_e \rightarrow \sqrt{1 - \eta_s} \nu_x + \sqrt{\eta_s} \nu_s. \quad (2.1)$$

The parameter  $\eta_s$  with  $0 \leq \eta_s \leq 1$  describes the fraction of the sterile neutrino participating in the solar oscillations. Therefore, the oscillation probabilities depend on the three parameters  $\Delta m_{\text{SOL}}^2$ ,  $\theta_{\text{SOL}}$  and  $\eta_s$ . The natural framework of light sterile neutrinos participating in oscillations are four-neutrino mass schemes, proposed to account for the LSND result [21] in addition to solar and atmospheric neutrino oscillations. For previous studies of solar neutrino oscillation in a four-neutrino framework see Refs. [20, 30, 31] and for an exact definition of the solar parameters and adopted approximations see Ref. [22].

### 2.2 Data and analysis

As experimental data, we use the solar neutrino rates of the chlorine experiment Homestake [2] ( $2.56 \pm 0.16 \pm 0.16$  SNU), the most recent result of the gallium experiments SAGE [3] ( $70.8^{+5.3}_{-5.2} {}^{+3.7}_{-3.2}$  SNU) and GALLEX/GNO [4] ( $73.3 \pm 4.7 \pm 4.0$  SNU), as well as the 1496-days Super-Kamiokande data sample [1] in the form of 44 bins (8 energy bins, 6 of which are further divided into 7 zenith angle bins). In addition to this, we include the latest results from SNO presented in Refs. [6, 7], in the form of 34 data bins (17 energy bins for each day and night period). Therefore, in our statistical analysis we use  $3 + 44 + 34 = 81$  observables, which we fit in terms of the three parameters  $\Delta m_{\text{SOL}}^2$ ,  $\theta_{\text{SOL}}$  and  $\eta_s$ , with a  $\chi^2_{\text{SOL}}$  of the form

$$\chi^2_{\text{SOL}}(\Delta m_{\text{SOL}}^2, \theta_{\text{SOL}}, \eta_s) = \sum_{i,j=1}^{81} (R_i^{\text{ex}} - R_i^{\text{th}}) \cdot (\sigma_{\text{ex}}^2 + \sigma_{\text{th}}^2)_{ij}^{-1} \cdot (R_j^{\text{ex}} - R_j^{\text{th}}). \quad (2.2)$$

In order to fully isolate the impact of the recent neutral current, spectral and day/night information of the SNO result, we also present an analysis which does not include such information. To this aim we use only the SNO events with energy higher than 6.75 MeV, for which the NC component is negligible [5]. We sum these events to a single rate, combining with Cl, Ga rates and full Super-K data, as described above. This procedure is analogous to the pre-SNO-NC situation, except that we take advantage of the enhanced statistics on the CC rate provided by the new data. We will refer to this analysis as SNO<sub>CC</sub><sup>rate</sup> analysis

and it contains 48 data points. The comparison with the analysis including the complete SNO data published this year ( $\text{SNO}_{\text{CC,NC}}^{\text{SP,DN}}$ ) allows us to highlight the impact of the SNO NC, spectral and day/night information.

For the solar neutrino fluxes we use the Standard Solar Model fluxes [32], including its standard  ${}^8\text{B}$  flux prediction<sup>1</sup>. Motivated by the excellent agreement of the recent SNO-NC result with the predictions of the Standard Solar Model, we prefer to adopt a boron-fixed analysis. We have checked that a boron-free analysis gives very similar results (see also Ref. [24]), even for non-zero  $\eta_s$ . For simplicity we neglect the *hep* and *F* neutrino fluxes, whose contribution to the present solar neutrino experiments is marginal.

For the neutrino cross sections of Chlorine, SAGE, GALLEX/GNO and Super-K we assume the same as used in previous papers [34, 35, 36], while for the CC and NC neutrino deuteron differential cross sections relevant for SNO we use the tables given in [37]. The contribution of the cross-section uncertainties to the covariance matrix for the Chlorine and Gallium experiments is calculated as suggested in Ref. [38]. For a given experiment (Chlorine or Gallium) we use full correlation of the error on the cross section for low-energy neutrino fluxes (*pp*, *pep*, *Be*, *N* and *O*), but no correlation of the cross section error between the low-energy fluxes and the higher-energy  ${}^8\text{B}$  flux.

The neutrino survival probability  $P_{ee}$  is extracted from the neutrino evolution operator  $\mathbf{U}$ , which we factorize as a product of three factors  $\mathbf{U}_{\text{sun}}$ ,  $\mathbf{U}_{\text{vac}}$  and  $\mathbf{U}_{\text{earth}}$  corresponding to propagation in the Sun, vacuum, and Earth, respectively. The first and last factors include matter effects with the corresponding density profiles given in Refs. [32] and [39]. As a simplifying approximation, we assume that  $\mathbf{U}_{\text{sun}}$  depends only on the neutrino production point  $\vec{x}_0$ ,  $\mathbf{U}_{\text{vac}}$  only on the Sun-Earth distance  $L$  and  $\mathbf{U}_{\text{earth}}$  depends only on the zenith-angle  $\zeta$  of the incoming neutrinos. Therefore in our calculations we neglect the small correlation between seasonal effects and day-night asymmetry [40]. For each value of the neutrino oscillation parameters  $\Delta m_{\text{SOL}}^2/E$ ,  $\theta_{\text{SOL}}$  and  $\eta_s$  we calculate the neutrino survival probability  $P_{ee}$  by averaging over  $\vec{x}_0$ ,  $L$  and  $\zeta$ , properly accounting for all the interference terms between  $\mathbf{U}_{\text{sun}}$ ,  $\mathbf{U}_{\text{vac}}$  and  $\mathbf{U}_{\text{earth}}$ .

Special care is taken in including all the theoretical and experimental errors and their cross-correlations in the calculation of the covariance matrix, for which we follow the description of Ref. [29] (covariance approach). In particular, the errors associated to the Boron-flux shape, the energy-scale and the energy-resolution uncertainties of the Super-Kamiokande and SNO experiments are recalculated for each point in parameter space.

---

<sup>1</sup>We choose not to include the flux indicated by the recent  $S_{17}$  measurement of Ref. [33].

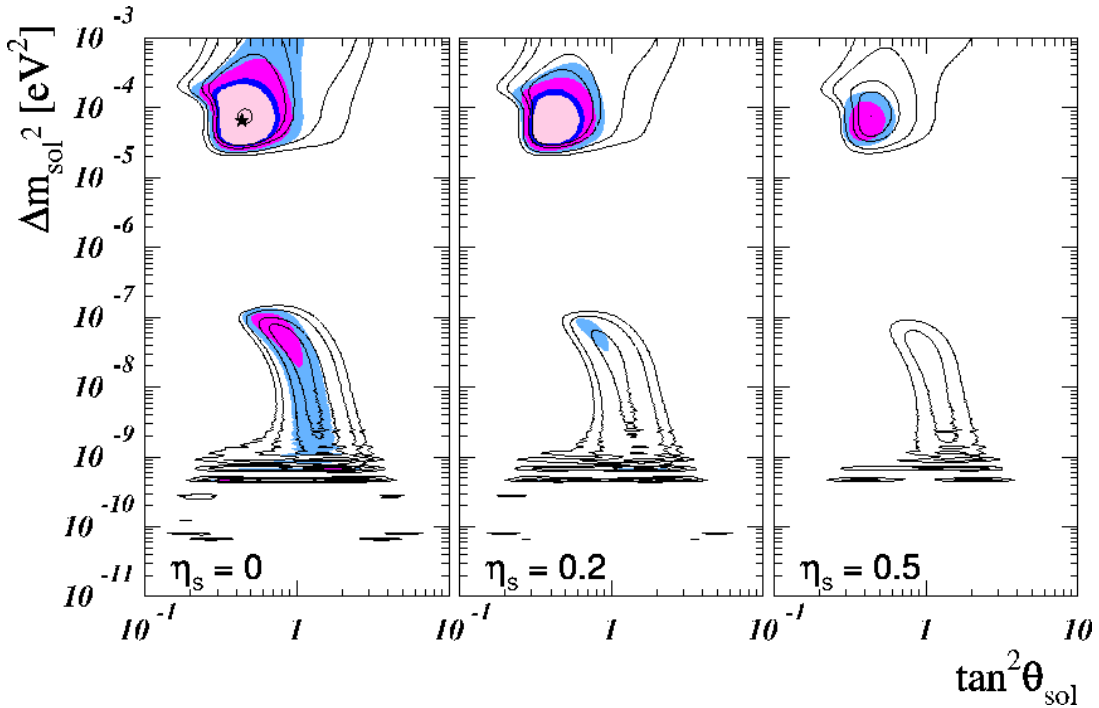


**Figure 1:** Allowed regions of  $\tan^2 \theta_{\text{sol}}$  and  $\Delta m_{\text{sol}}^2$  for  $\eta_s = 0$  (active oscillations),  $\eta_s = 0.2$  and  $\eta_s = 0.5$ . The lines indicate the regions determined by the  $\text{SNO}_{\text{CC}}^{\text{rate}}$  analysis (see definition in text), the shaded regions correspond to  $\text{SNO}_{\text{CC},\text{NC}}^{\text{SP},\text{DN}}$  (see text). The confidence levels are 90%, 95%, 99% and  $3\sigma$  for 3 d.o.f..

### 2.3 Results and discussion

In order to determine the expected event numbers for the various solar neutrino experiments we calculate the  $\nu_e$  survival probability for each point in parameter space of  $(\tan^2 \theta_{\text{sol}}, \Delta m_{\text{sol}}^2, \eta_s)$  and convolute it with the Standard Solar Model neutrino fluxes [32] and the relevant neutrino cross sections. We have compared such expected event numbers with the data described above, taking into account the detector characteristics and appropriate response functions. Using the above-mentioned  $\chi_{\text{sol}}^2$  we have performed a global fit of solar neutrino data, whose results we now summarize.

Our global best fit point occurs for the values

$$\tan^2 \theta_{\text{sol}} = 0.44, \quad \Delta m_{\text{sol}}^2 = 6.6 \times 10^{-5} \text{ eV}^2 \quad (2.3)$$

and correspond to  $\eta_s = 0$ . We obtain a  $\chi_{\text{min}}^2 = 66.1$  for  $81 - 3$  d.o.f., leading to the excellent goodness of fit of 83%. In Fig. 1 we display the regions of solar neutrino oscillation parameters for 3 d.o.f. with respect to this global minimum, for the standard case of active oscillations,  $\eta_s = 0$ , as well as for  $\eta_s = 0.2$  and  $\eta_s = 0.5$ . The first thing to notice is the impact of the SNO NC, spectral, and day/night data in improving the determination of

the oscillation parameters: the shaded regions after their inclusion are much smaller than the hollow regions delimited by the corresponding  $\text{SNO}_{\text{CC}}^{\text{rate}}$  confidence contours. Especially important is the full  $\text{SNO}_{\text{CC},\text{NC}}^{\text{SP},\text{DN}}$  information in closing the LMA region from above. Values of  $\Delta m_{\text{SOL}}^2 > 10^{-3} \text{ eV}^2$  appear only at  $3\sigma$ . Previously solar data on its own could not close the LMA region, only the inclusion of data from reactor experiments [14] ruled out the upper part of the LMA region [35]. Furthermore, the complete  $\text{SNO}_{\text{CC},\text{NC}}^{\text{SP},\text{DN}}$  information is important for excluding **maximal** solar mixing in the LMA region. At  $3\sigma$  we find the upper bound (1 d.o.f.):

$$\text{LMA} : \quad \tan^2 \theta_{\text{SOL}} \leq 0.83. \quad (2.4)$$

In order to compare our allowed regions given in Fig. 1 with those of other groups, one has to take into account that we calculate the C.L. regions for the 3 d.o.f.  $\tan^2 \theta_{\text{SOL}}$ ,  $\Delta m_{\text{SOL}}^2$  and  $\eta_s$ . Therefore at a given C.L. our regions are larger than the usual regions for 2 d.o.f., because we also constrain the parameter  $\eta_s$ .

Next we notice the enhanced discrimination against non-LMA solutions implied by the new data, apparent in Figs. 1, 2 and 3. This shows that the first hints [34] in favor of a globally preferred LMA oscillation solution which followed mainly from the flatness of the Super-K spectra, have now become a robust result, thanks to the additional data, to which SNO has contributed significantly<sup>2</sup>. One sees that, in contrast with the  $\text{SNO}_{\text{CC}}^{\text{rate}}$  situation, non-LMA solutions do not appear at 95% C.L.. However, the LOW and VAC solutions still appear at 99% C.L. for 3 d.o.f..

In order to concisely illustrate the above results we display in Fig. 2 the profiles of  $\Delta\chi_{\text{SOL}}^2$  as a function of  $\Delta m_{\text{SOL}}^2$  (left) as well as  $\tan^2 \theta_{\text{SOL}}$  (right), by minimizing with respect to the undisplayed oscillation parameters, for the fixed values of  $\eta_s = 0, 0.5, 1$ . By comparing top and bottom panels in Fig. 2 one can clearly see the impact of the full  $\text{SNO}_{\text{CC},\text{NC}}^{\text{SP},\text{DN}}$  sample in leading to the relative worsening of all non-LMA solutions with respect to the preferred active LMA solution.

The corresponding best fit values for the various solutions of  $\Delta m_{\text{SOL}}^2$  and  $\theta_{\text{SOL}}$  and the values of  $\chi_{\text{SOL}}^2$  evaluated at the best fit points are compiled in Tab. 1. This table gives results for the three cases considered above: pure active, pure sterile and mixed neutrino oscillations, both for the  $\text{SNO}_{\text{CC}}^{\text{rate}}$  and the  $\text{SNO}_{\text{CC},\text{NC}}^{\text{SP},\text{DN}}$  analysis. To calculate the goodness of fit of the various solutions we evaluate in this table the  $\chi^2$  for  $48 - 2$  ( $81 - 2$ ) d.o.f. for the  $\text{SNO}_{\text{CC}}^{\text{rate}}$  ( $\text{SNO}_{\text{CC},\text{NC}}^{\text{SP},\text{DN}}$ ) analysis defined previously. Note that we fix  $\eta_s$  at the three values 0, 0.5 and 1. In the pure active case we find for LOW, VAC and SMA the following

---

<sup>2</sup>See also Ref. [41].

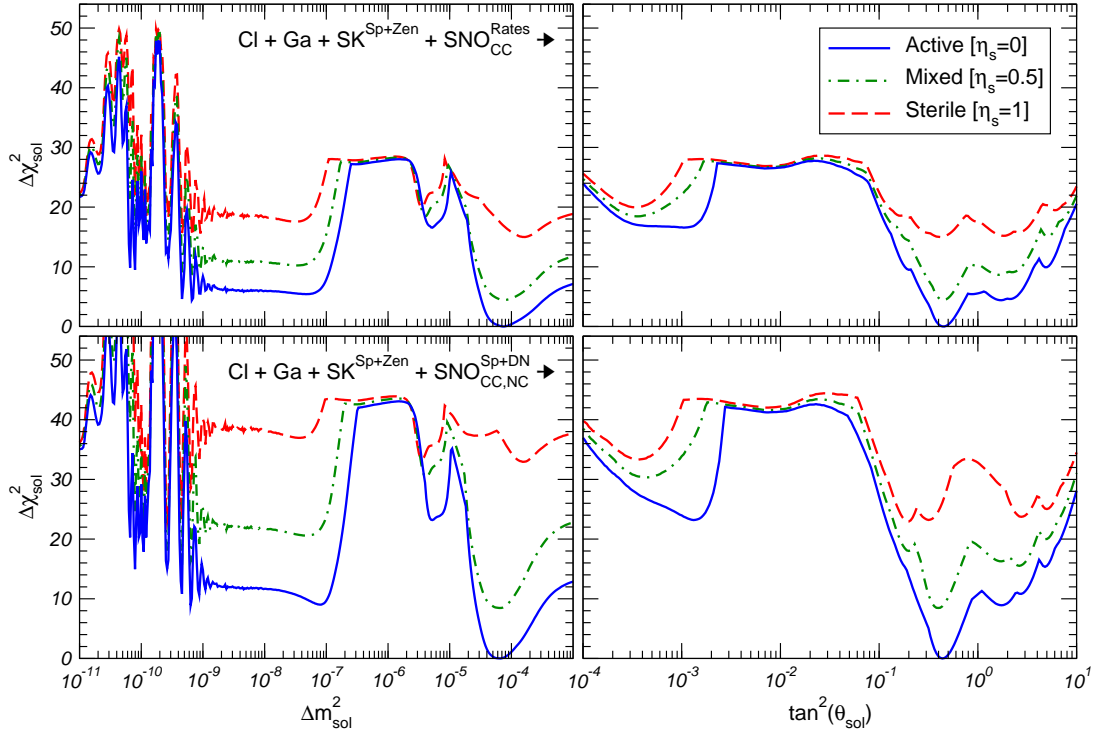


**Figure 2:**  $\Delta\chi^2_{\text{sol}}$  as a function of  $\Delta m_{\text{sol}}^2$  and  $\tan^2 \theta_{\text{sol}}$ , for pure active ( $\eta_s = 0$ ), pure sterile ( $\eta_s = 1$ ) and mixed neutrino oscillations ( $\eta_s = 0.5$ ). Upper and lower panels correspond to the  $\text{SNO}_{\text{CC}}^{\text{rate}}$  and  $\text{SNO}_{\text{CC,NC}}^{\text{SP, DN}}$  samples defined in text.

differences in  $\chi^2$  relative to the global best fit in LMA

$$\Delta\chi^2_{\text{LOW}} = 9.0, \quad \Delta\chi^2_{\text{VAC}} = 8.9, \quad \Delta\chi^2_{\text{SMA}} = 23.2. \quad (2.5)$$

Note that especially SMA is highly disfavoured with respect to LMA.

In addition to the scrutiny of the different neutrino oscillation solutions in the solar neutrino oscillation parameters  $\Delta m_{\text{sol}}^2$  and  $\theta_{\text{sol}}$ , the present solar data can test the sterile neutrino oscillation hypothesis, characterized by the parameter  $\eta_s$  introduced above. The results can be presented in several equivalent ways. For example, rejection of sterile solar neutrino oscillations is already hinted by comparing the middle and right panels of Fig. 1 with the left one, corresponding to the pure active oscillation case: clearly the solutions deteriorate as  $\eta_s$  increases. Furthermore, the lines for  $\eta_s = 0.5$  and  $\eta_s = 1$  shown in Fig. 2 clearly show that sterile solutions are strongly disfavoured with respect to pure active solutions.

In order to concisely illustrate the above results we display in Fig. 3 the profile of  $\Delta\chi^2_{\text{sol}}$  as a function of  $0 \leq \eta_s \leq 1$ , irrespective of the detailed values of the solar neutrino oscillation parameters  $\Delta m_{\text{sol}}^2$  and  $\theta_{\text{sol}}$ . This figure clearly illustrates the degree with which

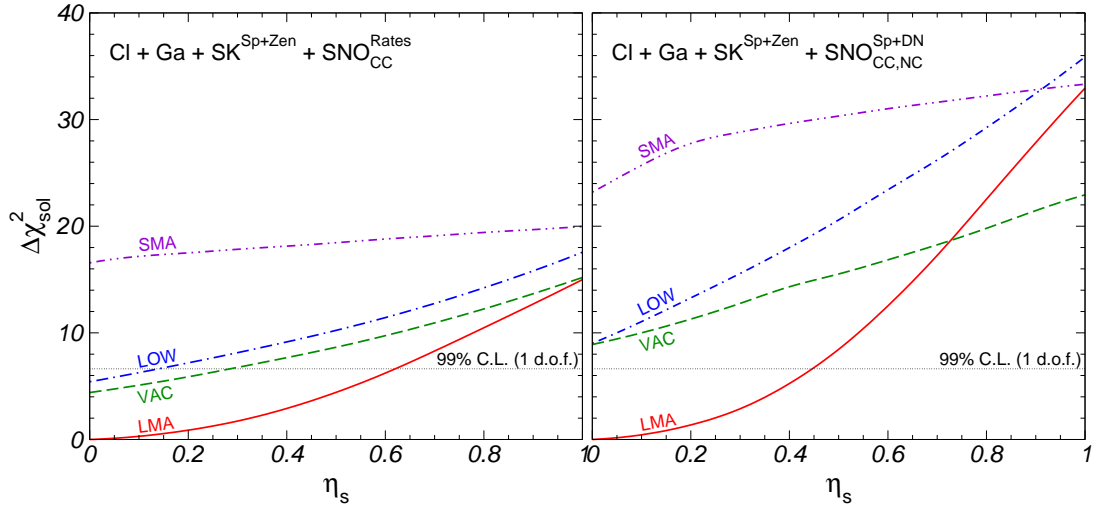


**Figure 3:**  $\Delta\chi^2_{\text{sol}}$  displayed as a function of  $\eta_s$  with respect to favored active LMA solution, for the  $\text{SNO}_{\text{CC}}^{\text{rate}}$  (left panel) and the  $\text{SNO}_{\text{CC},\text{NC}}^{\text{SP},\text{DN}}$  (right panel) analysis, as defined in text.

the solar neutrino data sample rejects the presence of a sterile component for each one of the possible solar neutrino oscillation solutions. The figure shows how the preferred LMA status survives in the presence of a small sterile component characterized by  $\eta_s$  (also seen in Figs. 1 and 2). Further, one sees that increasing  $\eta_s$  leads to a deterioration of all oscillation solutions. Notice that there is a crossing between the LMA and VAC solutions, as a result of which the best pure sterile description lies in the vacuum regime. However, in the global analysis pure sterile oscillations with  $\eta_s = 1$  are highly disfavored. We find a  $\chi^2$ -difference between pure active and sterile of  $\Delta\chi^2_{\text{s-a}} = 32.9$  if we restrict to the LMA solution, or  $\Delta\chi^2_{\text{s-a}} = 22.9$  if we allow also for VAC. For 3 d.o.f. the  $\Delta\chi^2_{\text{s-a}} = 22.9$  implies that pure sterile oscillations are ruled out at 99.996% C.L. compared to the active case. From the figure we obtain the bound

$$\text{solar data: } \eta_s \leq 0.45. \quad (2.6)$$

at 99% C.L. for 1 d.o.f.. In summary, we have found that, as long as the admixture of sterile neutrinos is acceptably small, the LMA is always the best of the oscillation solutions, establishing its robustness also in our generalized oscillation scheme.

To round off our discussion of the solar neutrino fit update we present in Fig. 4 the  $\nu_e$  survival probability versus energy  $E$  for the various solutions LMA, LOW and VAC, calculated as described above at the local  $\chi^2$ -minima given in Tab. 1. Similarly, plots can be made for the case of sterile oscillations.

Before turning to the atmospheric neutrino fits let us compare our solar neutrino results with the one of other groups. There have been several recent analyses in the

Region	SNO <sub>CC</sub> <sup>rate</sup>				SNO <sub>CC,NC</sub> <sup>SP, DN</sup>			
	$\tan^2 \theta_{\text{SOL}}$	$\Delta m_{\text{SOL}}^2$	$\chi^2_{\text{SOL}}$	g.o.f.	$\tan^2 \theta_{\text{SOL}}$	$\Delta m_{\text{SOL}}^2$	$\chi^2_{\text{SOL}}$	g.o.f.
Pure active ( $\eta_s = 0$ )								
LMA	0.46	$7.6 \times 10^{-5}$	41.3	67%	0.44	$6.6 \times 10^{-5}$	66.1	85%
LOW	0.87	$4.8 \times 10^{-8}$	46.7	44%	0.66	$7.9 \times 10^{-8}$	75.1	60%
VAC	1.7	$6.6 \times 10^{-10}$	45.7	49%	1.7	$6.3 \times 10^{-10}$	75.0	61%
SMA	$1.0 \times 10^{-3}$	$5.2 \times 10^{-6}$	57.9	11%	$1.3 \times 10^{-3}$	$5.2 \times 10^{-6}$	89.3	20%
Mixed ( $\eta_s = 0.5$ )								
LMA	0.44	$7.6 \times 10^{-5}$	45.7	48%	0.40	$6.6 \times 10^{-5}$	74.6	62%
LOW	0.95	$3.5 \times 10^{-8}$	51.5	27%	0.87	$4.8 \times 10^{-8}$	86.7	26%
VAC	1.7	$6.9 \times 10^{-10}$	49.9	32%	2.6	$4.6 \times 10^{-10}$	81.6	40%
SMA	$3.5 \times 10^{-4}$	$4.0 \times 10^{-6}$	59.7	8%	$4.2 \times 10^{-4}$	$4.2 \times 10^{-6}$	96.4	9%
Pure sterile ( $\eta_s = 1$ )								
LMA	0.42	$1.7 \times 10^{-4}$	56.3	14%	0.38	$1.5 \times 10^{-4}$	99.0	6%
LOW	1.0	$3.2 \times 10^{-8}$	58.8	10%	1.7	$1.1 \times 10^{-9}$	102.0	4%
VAC	1.8	$6.9 \times 10^{-10}$	56.5	14%	0.19	$2.6 \times 10^{-10}$	89.0	21%
SMA	$3.3 \times 10^{-4}$	$3.5 \times 10^{-6}$	61.3	7%	$3.6 \times 10^{-4}$	$3.5 \times 10^{-6}$	99.4	6%

**Table 1:** Best fit values of  $\Delta m_{\text{SOL}}^2$  and  $\theta_{\text{SOL}}$  with the corresponding  $\chi^2_{\text{SOL}}$  and GOF for pure active, pure sterile, and mixed neutrino oscillations. Results are given for the SNO<sub>CC</sub><sup>rate</sup> (left column) and the SNO<sub>CC,NC</sub><sup>SP, DN</sup> (right column) analysis. The relevant number of d.o.f. is 48 – 2 (81 – 2) for the SNO<sub>CC</sub><sup>rate</sup> (SNO<sub>CC,NC</sub><sup>SP, DN</sup>) analysis.

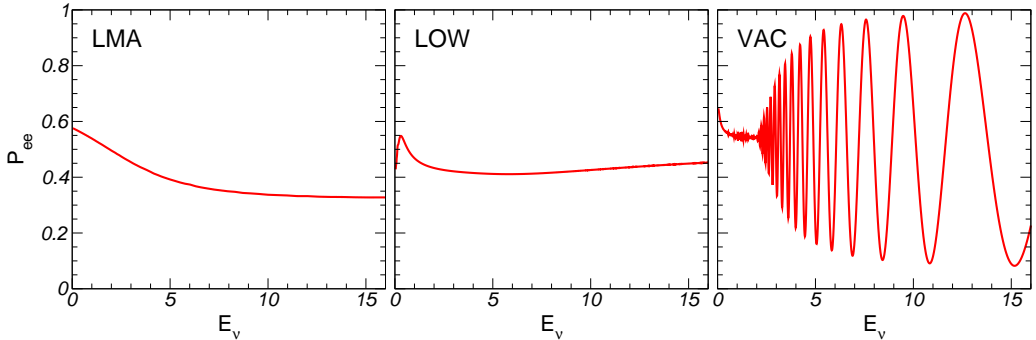


**Figure 4:** Best-fit active solar neutrino survival probabilities.

literature, however there has so far been no dedicated global analyses of solar neutrino data including the most recent SNO data, for the case where sterile neutrinos take part in solar oscillations ( $\eta_s \neq 0$ ). For the case of the preferred active LMA solution we find an excellent quantitative agreement with the results of the thorough analysis recently presented in Ref. [29]. Unfortunately in this reference only the case of active oscillations

$(\eta_s = 0)$  is considered. We also find good agreement with the results of other groups, e.g. Ref. [24, 25, 28], though not as quantitative, due to the differences in the analysis. For example, some of them include SNO and/or Super-K data in a different way. For the LMA case we also find good agreement with the results of Ref. [27]. In contrast, we find a sizable discrepancy with the results quoted in Ref. [26], especially regarding the SMA “solution”.

### 3. Atmospheric neutrinos

#### 3.1 Active-sterile atmospheric neutrino oscillations

In our analysis of atmospheric data we will make use of the hierarchy  $\Delta m_{\text{SOL}}^2 \ll \Delta m_{\text{ATM}}^2$  and neglect the solar mass splitting. Further, in order to comply with the strong constraints from reactor experiments [14] we completely decouple the electron neutrino from atmospheric oscillations<sup>3</sup>. In the following we will consider atmospheric neutrino data in a generalized oscillation scheme in which a light sterile neutrino takes part in the oscillations. The setting for such scenarios are four-neutrino mass schemes [15, 16, 17]. In such schemes, besides the solar and atmospheric mass-splittings, there is also a large  $\Delta m^2$  motivated by the LSND experiment [21]. In contrast with the case of solar  $\nu_e$  oscillations, the constraints on the  $\nu_\mu$ -content in atmospheric oscillations are not so stringent: in fact such constraints are provided by atmospheric data themselves [43]. As a result to describe atmospheric neutrino oscillations in this general framework [22, 31] we need two more parameters besides the standard 2-neutrino oscillation parameters  $\theta_{\text{ATM}}$  and  $\Delta m_{\text{ATM}}^2$ . We will use the parameters  $d_\mu$  and  $d_s$  already introduced in Ref. [22], and defined in such a way that  $1 - d_\mu$  ( $1 - d_s$ ) corresponds to the fraction of  $\nu_\mu$  ( $\nu_s$ ) participating in oscillations with  $\Delta m_{\text{ATM}}^2$ . Hence, pure active atmospheric oscillations with  $\Delta m_{\text{ATM}}^2$  are recovered in the limit  $d_\mu = 0$  and  $d_s = 1$ . In four-neutrino models there is a mass scheme-dependent relationship between  $d_s$  and the solar parameter  $\eta_s$ . For details see Ref. [22].

We will also perform an analysis by imposing the constraint  $d_\mu = 0$ . In such “restricted” analysis the  $\nu_\mu$  is completely constrained to the atmospheric mass states. Only in this limit the parameter  $d_s$  has a similar interpretation as  $\eta_s$  introduced in the solar case. For  $d_\mu = 0$  we obtain that  $\nu_\mu$  oscillates into a linear combination of  $\nu_\tau$  and  $\nu_s$  with  $\Delta m_{\text{ATM}}^2$ :

$$d_\mu = 0 : \quad \nu_\mu \rightarrow \sqrt{d_s} \nu_\tau + \sqrt{1 - d_s} \nu_s. \quad (3.1)$$

#### 3.2 Data and analysis

For the atmospheric data analysis we use all the charged-current data from the Super Kamiokande [12] and MACRO [13] experiments. The Super Kamiokande data include the

---

<sup>3</sup>For a dedicated study of these issues see Ref. [42].

$e$ -like and  $\mu$ -like data samples of sub- and multi-GeV contained events (10 bins in zenith angle), as well as the stopping (5 angular bins) and through-going (10 angular bins) up-going muon data events. We do not use the information on multi-ring  $\mu$  and neutral-current events since an efficient Monte-Carlo simulation of these data sample would require a more detailed knowledge of the Super Kamiokande experiment, and in particular of the way the neutral-current signal is extracted from the data. Such an information is presently not available to us. From MACRO we use the through-going muon sample divided in 10 angular bins [13].

Our statistical analysis of the atmospheric data is similar to that used in Ref. [22], except that we now take advantage of the new Super Kamiokande data and of the full ten-bin zenith-angle distribution for the contained events, rather than the five-bin distribution employed previously. Therefore, we have now 65 observables, which we fit in terms of the four relevant parameters  $\Delta m_{\text{ATM}}^2$ ,  $\theta_{\text{ATM}}$ ,  $d_\mu$  and  $d_s$ :

$$\chi_{\text{ATM}}^2(\Delta m_{\text{ATM}}^2, \theta_{\text{ATM}}, d_\mu, d_s) = \sum_{i,j=1}^{65} (N_i^{\text{ex}} - N_i^{\text{th}}) \cdot (\sigma_{\text{ex}}^2 + \sigma_{\text{th}}^2)_{ij}^{-1} \cdot (N_j^{\text{ex}} - N_j^{\text{th}}). \quad (3.2)$$

Concerning the theoretical Monte-Carlo, we improve the method presented in Ref. [35] by properly taking into account the scattering angle between the incoming neutrino and the scattered lepton directions. This was already the case for Sub-GeV contained events, however previously [22] we made the simplifying assumption of full neutrino-lepton collinearity in the calculation of the expected event numbers for the Multi-GeV contained and up-going- $\mu$  data samples. While this approximation is still justified for the stopping and thru-going muon samples, in the Multi-GeV sample the theoretically predicted value for down-coming  $\nu_\mu$  is systematically higher if full collinearity is assumed. The reason for this is that the strong suppression observed in these bins cannot be completely ascribed to the oscillation of the down-coming neutrinos (which is small due to small travel distance). Because of the non-negligible neutrino-lepton scattering angle at these Multi-GeV energies there is a sizable contribution from up-going neutrinos (with a higher conversion probability due to the longer travel distance) to the down-coming leptons. However, this problem is less visible when the angular information of Multi-GeV events is included in a five angular bins presentation of the data, as previously assumed [44].

### 3.3 Results and Discussion

Folding together the atmospheric neutrino fluxes [45], our calculated neutrino survival probabilities including Earth matter effects with the profile of Ref. [39], and the relevant neutrino cross sections, we determine the expected event numbers for the various atmospheric neutrino observables, taking into account the appropriate detector response

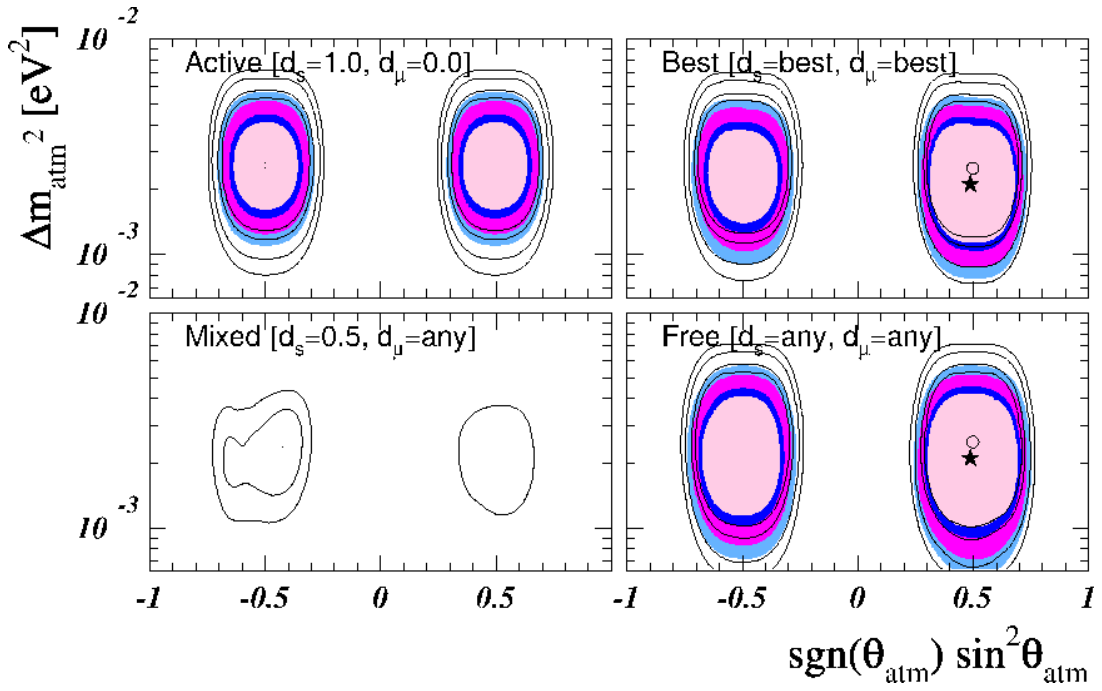


**Figure 5:** Allowed regions of the parameters  $\sin^2 \theta_{\text{ATM}}$  and  $\Delta m_{\text{ATM}}^2$  at 90%, 95%, 99% and  $3\sigma$  for 4 d.o.f. and different assumptions on the parameters  $d_s$  and  $d_\mu$  (see text). The lines (shaded regions) correspond to 1289 (1489) days of Super-K data.

characteristics. Comparing with the data described in Sec. 3.2, we have performed a global fit of the atmospheric neutrino data using the above-discussed  $\chi^2_{\text{ATM}}$ , following the same method used in Ref. [35]. We now summarize the main features of this fit.

Our global best fit point occurs at the parameter values

$$\sin^2 \theta_{\text{ATM}} = 0.49, \quad \Delta m_{\text{ATM}}^2 = 2.1 \times 10^{-3} \text{ eV}^2 \quad (\text{best}) \quad (3.3)$$

and  $d_s = 0.92$ ,  $d_\mu = 0.04$ . We see that atmospheric data prefers a small sterile neutrino admixture. However, this effect is not statistically significant, also the pure active case ( $d_s = 1, d_\mu = 0$ ) gives an excellent fit: the difference in  $\chi^2$  with respect to the best fit point is only  $\Delta\chi^2_{\text{act-best}} = 3.3$ . For the pure active best fit point we obtain

$$\sin^2 \theta_{\text{ATM}} = 0.5, \quad \Delta m_{\text{ATM}}^2 = 2.5 \times 10^{-3} \text{ eV}^2 \quad (\text{active}) \quad (3.4)$$

with the  $3\sigma$  ranges (1 d.o.f.)

$$0.3 \leq \sin^2 \theta_{\text{ATM}} \leq 0.7, \quad 1.2 \times 10^{-3} \text{ eV}^2 \leq \Delta m_{\text{ATM}}^2 \leq 4.8 \times 10^{-3} \text{ eV}^2 \quad (\text{active}) . \quad (3.5)$$

The determination of the parameters  $\theta_{\text{ATM}}$  and  $\Delta m_{\text{ATM}}^2$  is summarized in Figs. 5 and 6. At a given C.L. we cut the  $\chi^2_{\text{ATM}}$  at a  $\Delta\chi^2$  determined by 4 d.o.f. to obtain 4-dimensional

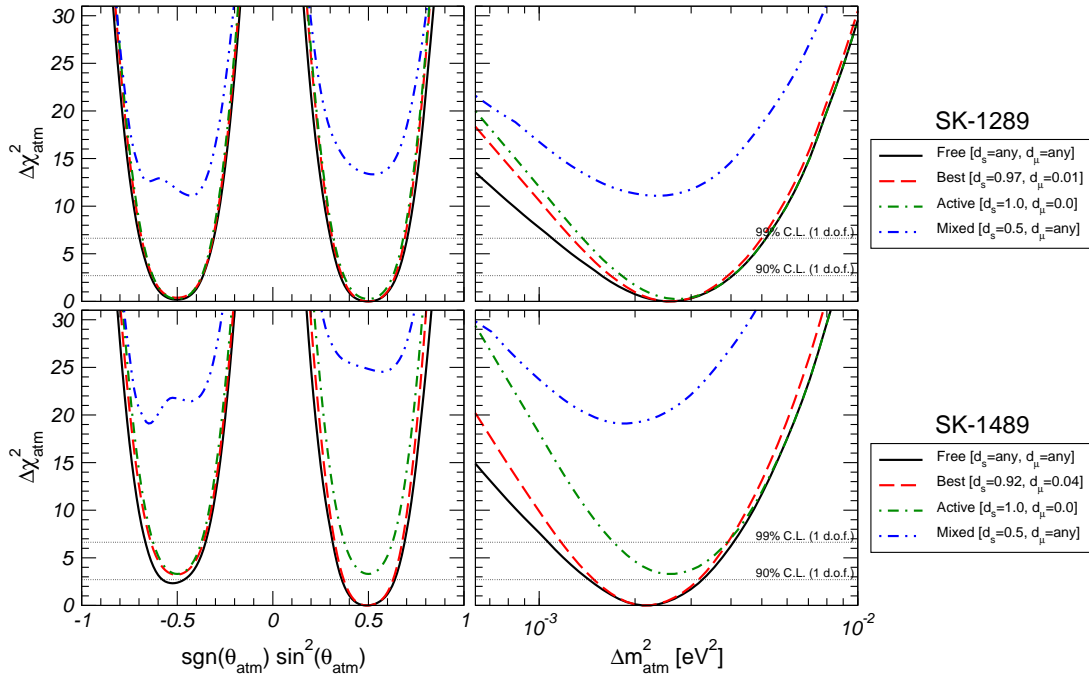


**Figure 6:**  $\Delta\chi^2_{\text{atm}}$  as a function of  $\sin^2 \theta_{\text{atm}}$  (left) and  $\Delta m^2_{\text{atm}}$  (right), using 1289 (upper) and 1489 (lower) days of Super-K data, for the case of neutrino oscillations with arbitrary  $d_s$  and  $d_\mu$ , best-fit  $d_s$  and  $d_\mu$ , pure active and mixed active-sterile neutrino oscillations.

volumes in the parameter space of  $(\theta_{\text{atm}}, \Delta m^2_{\text{atm}}, d_\mu, d_s)$ . In the upper panels we show sections of these volumes at values of  $d_s = 1$  and  $d_\mu = 0$  corresponding to the pure active case (left) and at the best fit point (right). Again we observe that moving from pure active to the best fit does not change the fit significantly. In the lower right panel we project away both  $d_\mu$  and  $d_s$ , whereas in the lower left panel we fix  $d_s = 0.5$  and project away only  $d_\mu$ . Comparing the regions resulting from 1489 days Super-K data (shaded regions) with the one from the 1289 days Super-K sample (hollow regions) we note that the new data leads to a slightly better determination of  $\theta_{\text{atm}}$  and  $\Delta m^2_{\text{atm}}$ . However, more importantly, from the lower left panel we see, that the new data shows a stronger rejection against a sterile admixture: for  $d_s = 0.5$  no allowed region appears at  $3\sigma$  for 4 d.o.f..

In Fig. 6 we display the  $\Delta\chi^2$  with respect to the global best fit point as a function of  $\sin^2 \theta_{\text{atm}}$  (for both signs of  $\theta_{\text{atm}}$ ) and  $\Delta m^2_{\text{atm}}$ , minimizing with respect to the other parameter, for different assumptions on the parameters  $d_s$  and  $d_\mu$ . In contrast to the solar case shown in Fig. 2 the atmospheric  $\chi^2$  exhibits a beautiful quadratic behaviour, reflecting the high quality of the fit and the robustness of the oscillation solution. Notice again the significant worsening of the fit for the case of a sizable sterile neutrino admixture (see, e. g. the line corresponding to  $d_s = 0.5$ ).

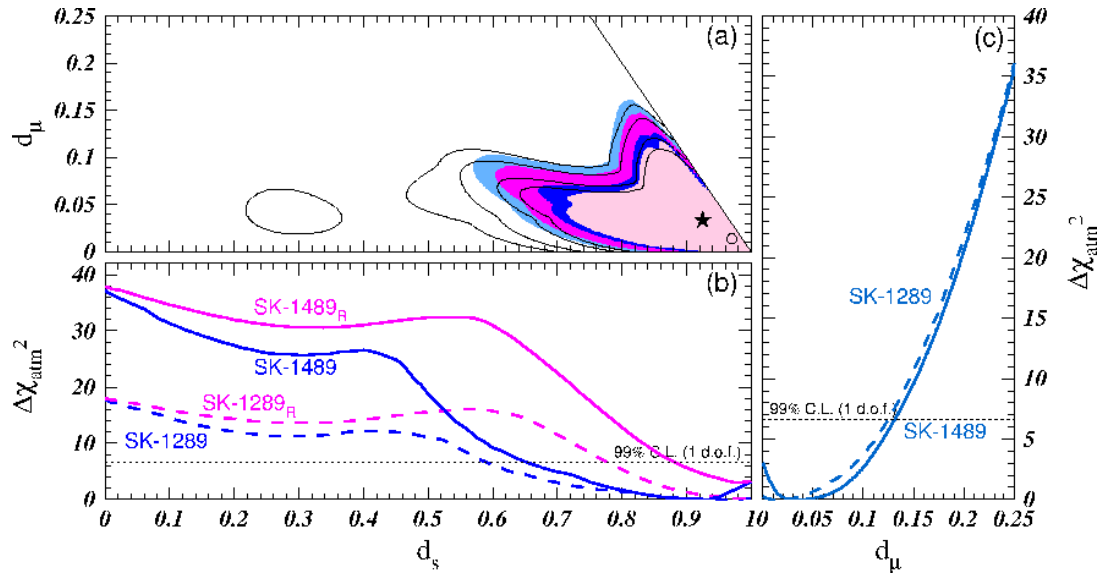


**Figure 7:** (a) Allowed regions of the parameters  $d_s$  and  $d_\mu$  at 90%, 95%, 99% and  $3\sigma$  for 2 d.o.f.. The lines (shaded regions) correspond to 1289 (1489) days Super-K data. Further we show  $\Delta\chi^2_{\text{atm}}$  as a function of  $d_s$  (b) and  $d_\mu$  (c), minimized with respect to all other parameters. The subscript “R” refers to the restricted analysis with  $d_\mu = 0$ .

In Fig. 7 we summarize the behaviour of atmospheric  $\chi^2$  with respect to the parameters  $d_s$  and  $d_\mu$ . Indeed, the most striking result of the present improved analysis is the stronger rejection we now obtain on the fraction of the sterile neutrino  $1 - d_s$  in atmospheric oscillations. Fig. 7 (b) clearly illustrates the degree with which the atmospheric neutrino data sample rejects the presence of a sterile component. On this basis one can place a model-independent atmospheric limit on the parameter  $d_s$ ,

$$\text{atmospheric data: } 1 - d_s \leq 0.35 \quad (3.6)$$

at 99% C.L.. For the case of the restricted analysis in which  $d_\mu = 0$  we obtain

$$d_\mu = 0 : \quad 1 - d_s \leq 0.16. \quad (3.7)$$

By comparing Eqs. (3.6) and (3.7) we note the importance of taking into account the finite  $d_\mu$  value in the analysis.

Although there is no substantial change in the 99% C.L. bounds on  $1 - d_s$  due to the new Super-K data there is a huge effect for the case of sizeable sterile neutrino admixtures,  $d_s \lesssim 0.5$ . In Tab. 2 we have compiled the best fit values of  $\sin^2 \theta_{\text{ATM}}$ ,  $\Delta m^2_{\text{ATM}}$ , the  $\chi^2$  values and the GOF for the various atmospheric data samples for pure active and pure sterile oscillations. In the last column we give the difference in  $\chi^2$  between active and sterile oscillation cases. Comparing these numbers for the 1289 and 1489 days Super-K samples

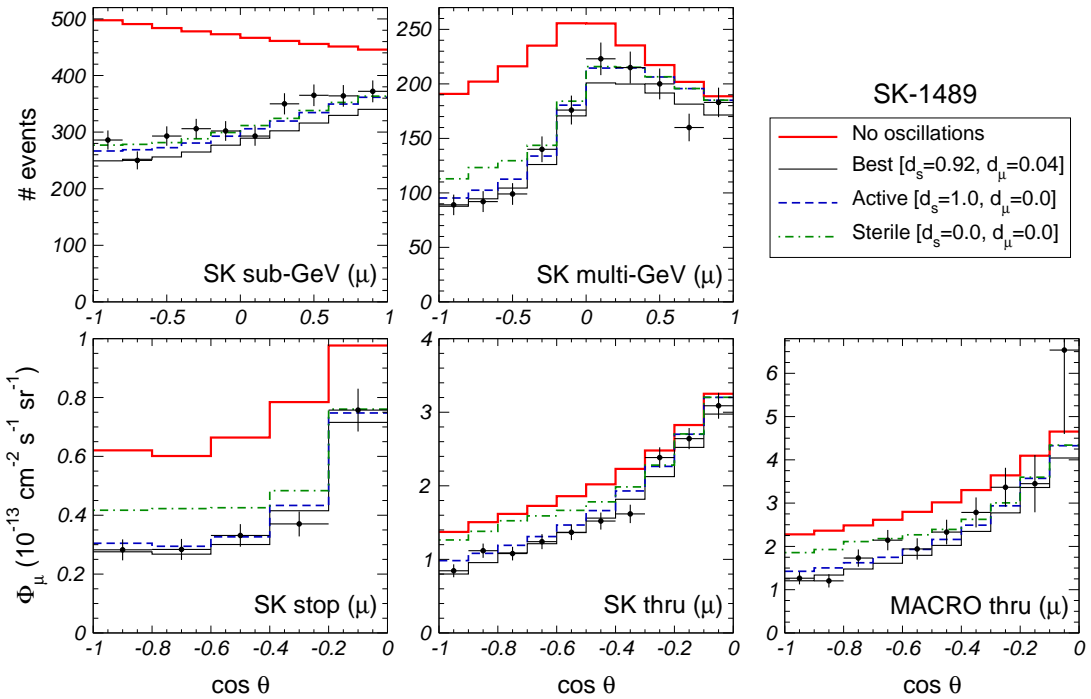


**Figure 8:** Zenith angle dependence of the  $\mu$ -like data used in our fit. Further we show the predicted number of atmospheric neutrino events for best-fit, pure-active and pure-sterile oscillations and no oscillations.

we observe that all the new data except the Sub-GeV sample lead to a significant higher rejection against sterile oscillations. In combination with MACRO data the 1289 days Super-K gave a difference between pure sterile and active oscillations of  $\Delta\chi^2_{s-a} = 17.8$ , whereas with the recent data we obtain

$$\Delta\chi^2_{s-a} = 34.6, \quad (3.8)$$

showing that pure sterile oscillations are highly disfavoured with respect to the active ones<sup>4</sup>. Let us note that MACRO data give an important contribution to this effect: MACRO alone disfavours the sterile oscillations already with  $\Delta\chi^2_{s-a} = 9.0$ . These limits on the sterile admixture are significantly stronger than obtained previously [22] and play an important role in ruling out four-neutrino oscillation solutions in a combined global analysis of the LSND anomaly [23]. Note, however, that in contrast with the case of  $d_s$ , there is no substantial improvement in constraining the parameter  $d_\mu$  due to the new data, as seen in Fig. 7 (c).

<sup>4</sup>This is in agreement with the analysis presented by Super-K at Neutrino 2002 [12]. By taking advantage of the full information accessible only inside the collaboration also multi-ring  $\mu$  and neutral-current events can be used to constrain sterile oscillations, leading to a value of  $\Delta\chi^2_{s-a} = 49.8$  [12].

Data sample	d.o.f.	Active ( $d_\mu = 0, d_s = 1$ )				Sterile ( $d_\mu = 0, d_s = 0$ )				$\Delta\chi^2_{s-a}$
		$\sin^2 \theta$	$\Delta m^2$ [eV $^2$ ]	$\chi^2_{\text{act}}$	g.o.f.	$\sin^2 \theta$	$\Delta m^2$ [eV $^2$ ]	$\chi^2_{\text{ste}}$	g.o.f.	
Super-K-1289 days, improved										
SK Sub-GeV	20 – 2	0.50	$2.1 \cdot 10^{-3}$	14.9	67%	0.50	$2.2 \cdot 10^{-3}$	15.0	66%	0.1
SK Multi-GeV	20 – 2	0.50	$1.8 \cdot 10^{-3}$	6.4	99%	0.57	$3.5 \cdot 10^{-3}$	11.3	88%	4.8
SK Stop- $\mu$	5 – 2	0.50	$4.2 \cdot 10^{-3}$	1.2	76%	0.61	$4.0 \cdot 10^{-3}$	3.1	38%	1.9
SK Thru- $\mu$	10 – 2	0.29	$6.3 \cdot 10^{-3}$	5.3	73%	0.84	$1.0 \cdot 10^{-2}$	7.8	45%	2.5
MACRO	10 – 2	0.50	$2.4 \cdot 10^{-3}$	11.0	20%	0.96	$9.4 \cdot 10^{-3}$	20.0	1%	9.0
SK Contained	40 – 2	0.50	$2.0 \cdot 10^{-3}$	21.4	99%	0.54	$3.0 \cdot 10^{-3}$	26.9	91%	5.5
Upgoing- $\mu$	25 – 2	0.50	$3.3 \cdot 10^{-3}$	19.2	69%	0.72	$4.2 \cdot 10^{-3}$	32.8	8%	13.6
SK+MACRO	65 – 2	0.50	$2.7 \cdot 10^{-3}$	41.7	98%	0.56	$2.8 \cdot 10^{-3}$	59.4	60%	17.8
Super-K-1489 days										
SK Sub-GeV	20 – 2	0.50	$1.9 \cdot 10^{-3}$	9.0	96%	0.51	$2.0 \cdot 10^{-3}$	9.0	96%	0.0
SK Multi-GeV	20 – 2	0.50	$1.3 \cdot 10^{-3}$	10.2	93%	0.57	$3.5 \cdot 10^{-3}$	18.4	43%	8.2
SK Stop- $\mu$	5 – 2	0.50	$2.8 \cdot 10^{-3}$	1.5	69%	0.75	$2.8 \cdot 10^{-3}$	6.9	8%	5.4
SK Thru- $\mu$	10 – 2	0.50	$3.5 \cdot 10^{-3}$	6.3	61%	0.84	$6.7 \cdot 10^{-3}$	16.0	4%	9.7
MACRO	10 – 2	0.50	$2.4 \cdot 10^{-3}$	11.0	20%	0.96	$9.4 \cdot 10^{-3}$	20.0	1%	9.0
SK Contained	40 – 2	0.50	$1.5 \cdot 10^{-3}$	19.3	99%	0.54	$3.0 \cdot 10^{-3}$	28.1	88%	8.8
Upgoing- $\mu$	25 – 2	0.50	$3.0 \cdot 10^{-3}$	18.9	71%	0.75	$3.2 \cdot 10^{-3}$	40.8	1%	22.0
SK+MACRO	65 – 2	0.50	$2.5 \cdot 10^{-3}$	40.2	99%	0.61	$2.7 \cdot 10^{-3}$	74.9	15%	34.6

**Table 2:** Atmospheric neutrino best-fit oscillation parameters for pure active and pure sterile oscillations for the various data samples.

In order to better appreciate the excellent quality of the neutrino oscillation description of the present atmospheric neutrino data sample we display in Fig. 8 the zenith angle distribution of atmospheric neutrino events. Clearly, active neutrino oscillations describe the data very well indeed. In contrast, no oscillations can be visually spotted as being inconsistent. On the other hand conversions to sterile neutrinos lead to an excess of events for neutrinos crossing the core of the Earth, in all the data samples except sub-GeV.

#### 4. Conclusions

Prompted by the recent data on solar and atmospheric neutrinos we have reanalised the global status of oscillation solutions, taking into account the that both the solar  $\nu_e$  and the atmospheric  $\nu_\mu$  may convert to a mixture of active and sterile neutrinos. In addition to the SNO neutral current, spectral and day/night ( $\text{SNO}_{\text{CC,NC}}^{\text{SP,DN}}$ ) results we add the latest 1496-day solar and 1489-day atmospheric Super-K neutrino data samples.

We have studied the impact of the recent solar data in the determination of the regions of oscillation parameters for different allowed  $\eta_s$  values, displaying the global behavior of  $\Delta\chi^2_{\text{SOL}}(\Delta m^2_{\text{SOL}})$  and  $\Delta\chi^2_{\text{SOL}}(\theta_{\text{SOL}})$ , calculated with respect to the favored active LMA solution. We have investigated in detail the impact of the full Cl + Ga rates + Super-K spectra + SNO<sub>CC,NC</sub><sup>SP, DN</sup> data, compared to the situation when this year's SNO data is left out. We confirm the clear preference for the LMA solution of the solar neutrino problem and obtain that the LOW, VAC, SMA solutions are disfavoured with a  $\Delta\chi^2 = 9, 9, 23$ , respectively. In addition, we find that the global solar data sample constrains admixtures of a sterile neutrino to be smaller than 45% at 99% C.L.. A pure sterile solution is ruled out with respect to the active one at 99.996% C.L.. For allowed sterile neutrino admixtures LMA is always the best of all the oscillation solutions. We remark, however, the existence of non-oscillation solutions [8, 9]. These will be crucially tested at the up-coming KamLAND reactor experiment [46].

By performing an improved fit of the atmospheric data, we have also updated the corresponding regions of oscillation parameters for the case where the atmospheric  $\nu_\mu$  convert to a mixture of active and sterile neutrinos. We have displayed the global behavior of  $\Delta\chi^2_{\text{ATM}}(\Delta m^2_{\text{ATM}})$  and  $\Delta\chi^2_{\text{ATM}}(\theta_{\text{ATM}})$  for different allowed values of the sterile neutrino admixture in the atmospheric channel. We have compared the situation before-and-after the recent 1489-day atmospheric Super-K data samples and shown that the GOF of the oscillation hypothesis is excellent. We have found that the recent 1489-day atmospheric Super-K data strongly constrain a sterile component in atmospheric oscillations: if the  $\nu_\mu$  is restricted to the atmospheric mass states only a sterile admixture of 16% is allowed at 99% C.L., while a bound of 35% is obtained in the unconstrained case. Pure sterile oscillations are disfavoured with a  $\Delta\chi^2 = 34.6$  compared to the active case.

## Acknowledgments

We thank Mark Chen, Andre Hamer, Art McDonald and Scott Oser, for help in accessing the details of the SNO experiment needed for our analysis. This work was supported by Spanish grant PB98-0693, by the European Commission RTN network HPRN-CT-2000-00148 and by the European Science Foundation network grant N. 86. T.S. has been supported by the DOC fellowship of the Austrian Academy of Science and, in the early stages of this work, by a fellowship of the European Commission Research Training Site contract HPMT-2000-00124 of the host group. M.M. was supported by contract HPMF-CT-2000-01008 and M.A.T. was supported by the M.E.C.D. fellowship AP2000-1953.

## References

- [1] M. Smy, talk at Neutrino 2002, <http://neutrino2002.ph.tum.de/> and arXiv:hep-ex/0202020; S. Fukuda *et al.* [Super-Kamiokande Collaboration], Phys. Lett. B **539** (2002) 179 [arXiv:hep-ex/0205075]. Super-Kamiokande Coll., Y. Fukuda *et al.*, Phys. Rev. Lett. **81**, 1158 (1998); Erratum *ibid.* **81**, 4279 (1998) and *ibid.* **82**, 1810 and 2430 (1999); Y. Suzuki, Nucl. Phys. B (Proc. Suppl.) **77**, 35 (1999); S. Fukuda *et al.*, hep-ex/0103032.
- [2] B.T. Cleveland *et al.*, Astrophys. J. **496**, 505 (1998); R. Davis, Prog. Part. Nucl. Phys. **32**, 13 (1994);
- [3] SAGE Coll., D.N. Abdurashitov *et al.*, Phys. Rev. **C60**, 055801 (1999); astro-ph/0204245.
- [4] GALLEX Coll., W. Hampel *et al.*, Phys. Lett. **B447**, 127 (1999); M. Altmann *et al.*, GNO Coll., Phys. Lett. B 490 (2000) 16, hep-ex/0006034; C. Cattadori, GNO Coll., Nucl. Phys. B (Proc. Suppl.) **110** (2002) 311.
- [5] Q. R. Ahmad *et al.* [SNO Collaboration], Phys. Rev. Lett. **87** (2001) 071301 [arXiv:nucl-ex/0106015].
- [6] Q. R. Ahmad *et al.* [SNO Collaboration], Phys. Rev. Lett. **89**, 011301 (2002) [arXiv:nucl-ex/0204008].
- [7] Q. R. Ahmad *et al.* [SNO Collaboration], Phys. Rev. Lett. **89**, 011302 (2002) [arXiv:nucl-ex/0204009].
- [8] O. G. Miranda *et al.*, Nucl. Phys. B **595** (2001) 360 [arXiv:hep-ph/0005259]. Phys. Lett. B **521** (2001) 299 [arXiv:hep-ph/0108145], and references therein.
- [9] M. Guzzo *et al.*, Nucl. Phys. B **629** (2002) 479 [arXiv:hep-ph/0112310], and references therein.
- [10] Y. Fukuda *et al.*, Kamiokande Coll., Phys. Lett. B **335** (1994) 237; R. Becker-Szendy *et al.*, IMB Coll., Nucl. Phys. B (Proc. Suppl.) **38** (1995) 331; W.W.M. Allison *et al.*, Soudan Coll., Phys. Lett. B **449** (1999) 137.
- [11] MACRO Coll., M. Ambrosio *et al.*, Phys. Lett. B **434** (1998) 451; M. Spurio *et al.*, hep-ex/0101019; B. Barish, Talk given at *Neutrino 2000*, 15–21 June 2000, Sudbury, Canada [<http://nu2000.sno.laurentian.ca>].

- [12] M. Shiozawa, talk at Neutrino 2002, <http://neutrino2002.ph.tum.de/>; Super-Kamiokande Coll., Y. Fukuda *et al.*, Phys. Rev. Lett. **81** (1998) 1562
- [13] A. Surdo, Talk given at *TAUP 2001*, 8–12 September 2001, Gran Sasso, Italy [<http://www.lngs.infn.it/>].
- [14] M. Apollonio *et al.*, CHOOZ Coll., Phys. Lett. B **466** (1999) 415; F. Boehm *et al.*, Palo Verde Coll., Phys. Rev. D **64** (2001) 112001 [hep-ex/0107009].
- [15] J. T. Peltoniemi, D. Tommasini and J. W. F. Valle, Phys. Lett. B **298** (1993) 383.
- [16] J. T. Peltoniemi and J. W. F. Valle, Nucl. Phys. B **406**, 409 (1993) [hep-ph/9302316].
- [17] D.O. Caldwell and R.N. Mohapatra, Phys. Rev. D **48** (1993) 3259.
- [18] A. Ioannian and J. W. F. Valle, Phys. Rev. D **63** (2001) 073002; R. N. Mohapatra, A. Perez-Lorenzana and C. A. de S Pires, Phys. Lett. B **491** (2000) 14.
- [19] M. Hirsch and J. W. F. Valle, Phys. Lett. B **495** (2000) 121 [hep-ph/0009066].
- [20] Web-page of C. Giunti, <http://www.to.infn.it/~giunti/neutrino/> .
- [21] C. Athanassopoulos *et al.*, LSND Coll., Phys. Rev. Lett. **77** (1996) 3082; *ibid* **81** (1998) 1774; A. Aguilar *et al.* [LSND Collaboration], Phys. Rev. D **64** (2001) 112007 [arXiv:hep-ex/0104049].
- [22] M. Maltoni, T. Schwetz and J. W. Valle, Phys. Rev. D **65** (2002) 093004 [arXiv:hep-ph/0112103].
- [23] M. Maltoni, T. Schwetz, M. A. Tórtola, and J. W. Valle, hep-ph/0207157
- [24] J.N. Bahcall et al. hep-ph/0204314
- [25] A. Bandyopadhyay et al. hep-ph/0204286
- [26] V. Barger et al. Phys.Lett. B537 (2002) 179-186 [hep-ph/0204253]
- [27] P.C. de Holanda, A.Yu. Smirnov hep-ph/0205241
- [28] P. Creminelli et al. hep-ph/0102234 (updated on 22 Apr 02 including the SNO NC and day/night results).
- [29] G. L. Fogli, E. Lisi, A. Marrone, D. Montanino and A. Palazzo, arXiv:hep-ph/0206162.
- [30] C. Giunti, M. C. Gonzalez-Garcia and C. Pena-Garay, Phys. Rev. D **62**, 013005 (2000).

- [31] M. C. Gonzalez-Garcia, M. Maltoni and C. Pena-Garay, Phys. Rev. D **64**, 093001 (2002).
- [32] Bahcall's page <http://www.sns.ias.edu/~jnb/> and references therein.
- [33] A. R. Junghans *et al.*, Phys. Rev. Lett. **88**, 041101 (2002) [arXiv:nucl-ex/0111014].
- [34] M. C. Gonzalez-Garcia, P. C. de Holanda, C. Pena-Garay and J. W. Valle, Nucl. Phys. B **573** (2000) 3 [arXiv:hep-ph/9906469].
- [35] M. C. Gonzalez-Garcia, M. Maltoni, C. Pena-Garay and J. W. F. Valle, Phys. Rev. D **63** (2001) 033005 [hep-ph/0009350]; N. Fornengo, M.C. Gonzalez-Garcia and J. W. F. Valle, Nucl. Phys. B **580** (2000) 58; M. C. Gonzalez-Garcia, H. Nunokawa, O. L. G. Peres and J. W. F. Valle, Nucl. Phys. B **543** (1999) 3 [hep-ph/9807305].
- [36] J. N. Bahcall, M. C. Gonzalez-Garcia and C. Pena-Garay, JHEP **0204**, 007 (2002) [arXiv:hep-ph/0111150].
- [37] K. Kubodera's web-page <http://nuc003.psc.sc.edu/~kubodera/>
- [38] J. N. Bahcall, M. C. Gonzalez-Garcia and C. Pena-Garay, arXiv:hep-ph/0204194.
- [39] A. M. Dziewonski and D. L. Anderson, Phys. Earth Planet. Inter. **25**, 297 (1981).
- [40] P. C. de Holanda, C. Pena-Garay, M. C. Gonzalez-Garcia and J. W. Valle, Phys. Rev. D **60**, 093010 (1999) [arXiv:hep-ph/9903473].
- [41] A. Strumia *et al.*, hep-ph/0205261.
- [42] M. C. Gonzalez-Garcia and M. Maltoni, arXiv:hep-ph/0202218.
- [43] M. Maltoni, T. Schwetz and J. W. Valle, Phys. Lett. B **518**, 252 (2001) [arXiv:hep-ph/0107150].
- [44] M. C. Gonzalez-Garcia, H. Nunokawa, O. L. Peres, T. Stanev and J. W. Valle, Phys. Rev. D **58** (1998) 033004 [arXiv:hep-ph/9801368].
- [45] G. Barr, T. K. Gaisser and T. Stanev, Phys. Rev. D **39** (1989) 3532; Phys. Rev. D **38** (1988) 85; T. K. Gaisser and T. Stanev, Phys. Rev. D **57**, 1977 (1998)
- [46] A. Piepke, KamLAND Coll., Nucl. Phys. B (Proc. Suppl.) **91**, 99 (2001); <http://kamland.lbl.gov/KamLAND>.